nature chemical engineering

Article

https://doi.org/10.1038/s44286-023-00004-2

Dynamic molecular pockets on one-dimensional channels for splitting ethylene from C_2–C_4 alkynes

Received: 13 September 2023

Accepted: 21 November 2023

Published online: 11 January 2024

Check for updates

Heng Zeng[1,2], Xiao-Jing Xie[1,2], Ting Wang[1,2], Mo Xie[1,2], Ying Wang[1,2], Rong-Jia Wei[1,2], Weigang Lu[1,2] ✉ & Dan Li[1,2] ✉

Molecular sieving adsorbents can offer maximum adsorption selectivity with respect to molecular sizes, yet it is still challenging to discriminate middle-sized molecules from a mixture of three or more components. Here we report a metal–organic framework (JNU-3a) with dynamic molecular pockets along one-dimensional channels, enabling the one-step removal of ethylene (C_2H_4) from mixtures with C_2–C_4 alkynes in a single adsorption step regardless of their molecular sizes. Laboratory-scale column breakthrough experiments on 1.4 g of JNU-3a reveal that the three alkynes break through the column at almost the same but a later time, resulting in the high-purity separation of C_2H_4 (≥99.9995%) from a mixture with C_2–C_4 alkynes in a single adsorption operation. We further demonstrate pilot-scale column breakthrough on 107 g of JNU-3a and the collection of C_2H_4 in a gas cylinder. In particular, 30 continuous runs for a C_2H_2/C_3H_4/1-C_4H_6/C_2H_4 mixture (1:1:1:97) afford an average of 76.1 g per cycle of high-purity C_2H_4. Overall, JNU-3a may have great potential for industrial C_2H_4 purification via the concurrent removal of C_2–C_4 alkynes.

Ethylene (C_2H_4) is one of the most important feedstocks for manufacturing valuable organic chemicals and polymers[1]. In 2019, over 200 million metric tonnes of C_2H_4 were produced through hydrocarbon cracking[2,3]. However, the obtained C_2H_4 inevitably contains trace amounts of alkynes, including acetylene (C_2H_2), propyne (C_3H_4) and 1-butyne (1-C_4H_6)[4], resulting in catalyst deactivation during C_2H_4 polymerization and an adverse effect on the quality of the resulting polyethylene[5]. These alkynes need to be reduced to a concentration below 5 ppm before the production of polyethylene because they cause irreversible catalyst poisoning through the formation of solid metal acetylides[6], which can block the fluid stream and lead to explosion[7]. The current industrial practice of removing trace alkynes from C_2H_4 is via performing selective hydrogenation using palladium-based catalysts, although such catalysts are of high cost and can enable undesired reactions[8].

Selective adsorption using porous materials has been deemed an energy-efficient technology for hydrocarbon separation[9,10]; however, for hydrocarbons with the same carbon chain length, the alkyne and the corresponding alkene differ by just two hydrogen atoms, and their separation efficiency hinges largely on precise control over the pore structures and sizes of the porous materials. In this regard, metal–organic frameworks (MOFs), also known as porous coordination polymers, stand out because of their tailor-made pore dimensions and surface chemistry, due to the versatility of their building blocks and the variety of connection modes[11–16]. MOF materials have been studied extensively as adsorbents for alkyne/alkene separations[17–20].

To enhance the alkyne/alkene selectivity, one of the often-applied strategies is surface engineering, to preferentially boost the binding affinity for the alkyne over the alkene[10,21–23]. For example, the benchmark C_2H_2-selective MOF material ZJU-74 (ref. 24) features a sandwich-like

[1]College of Chemistry and Materials Science, Jinan University, Guangzhou, People's Republic of China. [2]Guangdong Provincial Key Laboratory of Functional Supramolecular Coordination Materials and Applications, Jinan University, Guangzhou, People's Republic of China. ✉e-mail: weiganglu@jnu.edu.cn; danli@jnu.edu.cn

https://doi.org/10.1038/s44286-023-00004-2

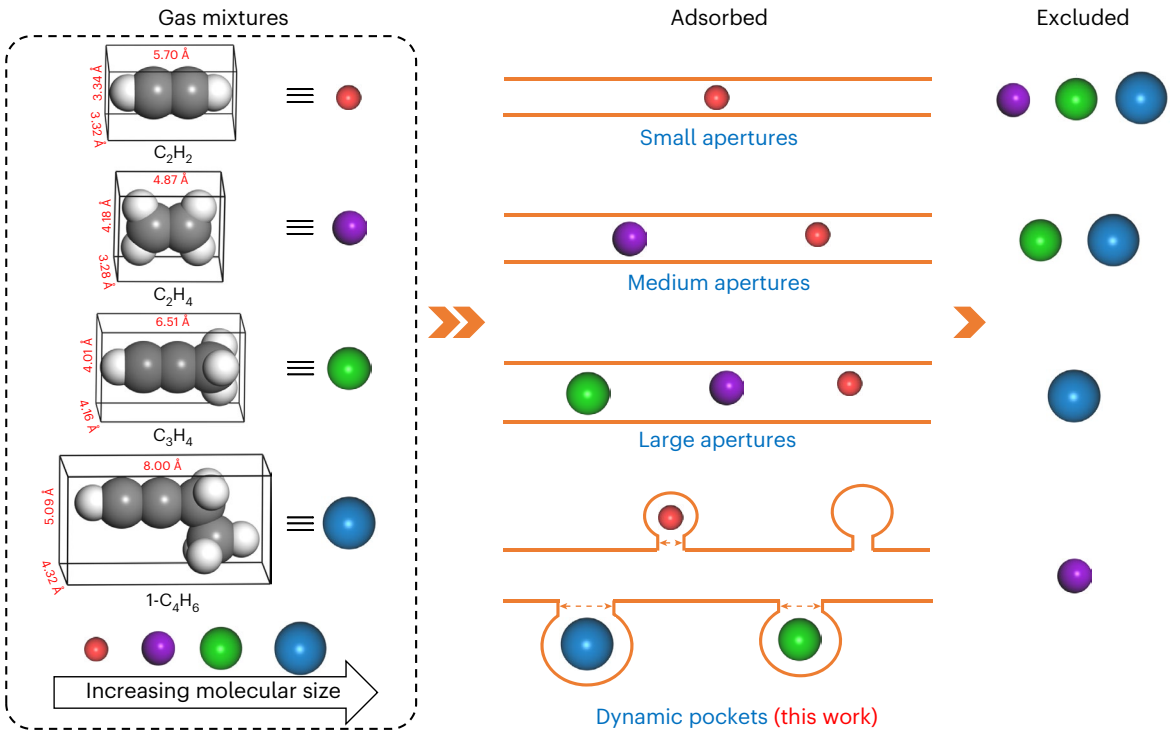

Fig. 1 | Adsorptive separation mechanism. Schematic illustration of orthogonal-array dynamic molecular pockets on a 1D channel for the one-step purification of C_2H_4 from a mixture with three alkynes regardless of their molecular sizes. Color code: C_2H_2, red; C_2H_4, purple; C_3H_4, green; 1-C_4H_6, blue; orange lines, pore structures.

structure with dual open metal sites (OMSs) per cluster and exhibits an ultrahigh C_2H_2 binding affinity (65 kJ mol^{-1}) and adsorption capacity (49 cm^3 g^{-1} at 0.01 bar and 296 K), resulting in a C_2H_2/C_2H_4 adsorption selectivity of 24.2. However, it should be pointed out that the alkyne/alkene selectivity based on such a strategy may be limited as OMSs also interact with the π-electrons of alkenes, as well as being sensitive to moisture.

Besides surface engineering, building small apertures is another commonly used strategy for alkyne/alkene separation. Ideally, such a structure design may result in minimum co-adsorption of the relatively large-sized alkene due to size exclusion and, therefore, high alkyne/alkene adsorption selectivity[25–27]. For example, using a shorter organic linker of 4,4′-azopyridine (9.0 Å) instead of 4,4′-dipyridylacetylene (9.6 Å), Chen and colleagues constructed a C_2H_2-sieving MOF material, SIFSIX-14-Cu-i (also known as UTSA-200)[26]. The contracted pore size (3.4 Å) of this MOF enables the complete exclusion of C_2H_4 with a C_2H_2/C_2H_4 adsorption selectivity of 6,320. Such a size-exclusion separation works well for binary gas mixtures, for example, C_2H_2/C_2H_4 (ref. 26) or C_3H_4/C_3H_6 (ref. 25), yet it will most probably fail to separate the middle-sized molecules from a mixture of three or more components in one separation step.

Flexible MOFs can offer unique opportunities for the separation of multicomponent mixtures because of their potential to discriminate guest molecules based on host–guest interactions rather than molecular dimensions[21,27–29]. For example, Zhang and co-workers reported a MOF material (MAF-41) with restricted flexibility[29] that functions as an intermediate-sized molecular sieve for adsorbing styrene while completely excluding the larger-sized ethylbenzene and smaller-sized toluene/benzene components. Moreover, further desorption is required to obtain the adsorbed styrene.

Here we report a robust MOF material (JNU-3a, named as the research was performed at Jinan University)[30] with orthogonal-array dynamic molecular pockets on one-dimensional (1D) channels to enable the production of high-purity C_2H_4 from its mixtures with C_2H_2, C_3H_4 and 1-C_4H_6 in a single adsorption step (Fig. 1). In situ single-crystal X-ray diffraction studies reveal the dynamic behavior of the molecular pocket on adsorbing C_2H_2, C_2H_4, C_3H_4 or 1-C_4H_6. The binding energy for the three alkynes is substantially higher than that for C_2H_4, as shown by their heats of adsorption that are either calculated from equilibrium adsorption data or measured using differential scanning calorimetry. Laboratory-scale column breakthrough experiments (using 1.4 g of JNU-3a) were conducted over a broad range of flow rates and even under humid conditions, and demonstrated the high separation capacity of JNU-3a for high-purity C_2H_4 from $C_2H_2/C_3H_4/1$-C_4H_6/C_2H_4 mixtures. We further demonstrate the collection of high-purity C_2H_4 (≥99.9995%) in a gas cylinder from a $C_2H_2/C_3H_4/1$-C_4H_6/C_2H_4 mixture (1:1:1:97) on a pilot-scale column breakthrough setup (using 107 g of JNU-3a), with an average collection of 76.1 g of C_2H_4 per run over 30 cycles. JNU-3a exhibits negligible competition between the three alkynes for the adsorption sites (molecular pockets), enabling the one-step direct production of high-purity C_2H_4 via the concurrent removal C_2H_2, C_3H_4 and 1-C_4H_6.

Results

Porosity analysis

The gram-scale synthesis of JNU-3 was carried out according to a previously reported method[30]. The desolvated JNU-3 (termed JNU-3a) retains the structural integrity of the 3D scaffold and features 1D narrow channels with an orthogonal array of molecular pockets on both sides (Supplementary Figs. 1 and 2). The pockets were observed to open up for propylene (C_3H_6) or propane (C_3H_8) through 'gourd shaped' apertures depending on the pressure[30], where the channel dimensions are approximately 4.5 × 5.3 Å^2 with a cross-sectional area of 23.85 Å^2, which is larger than the minimum cross-section of C_2H_2 (11.09 Å^2), C_2H_4 (13.71 Å^2), C_3H_4 (16.68 Å^2) or 1-C_4H_6 (21.90 Å^2) molecules (Supplementary Figs. 3 and 4); this prompted us to investigate further the gas adsorption behavior of JNU-3a for these hydrocarbons.

https://doi.org/10.1038/s44286-023-00004-2

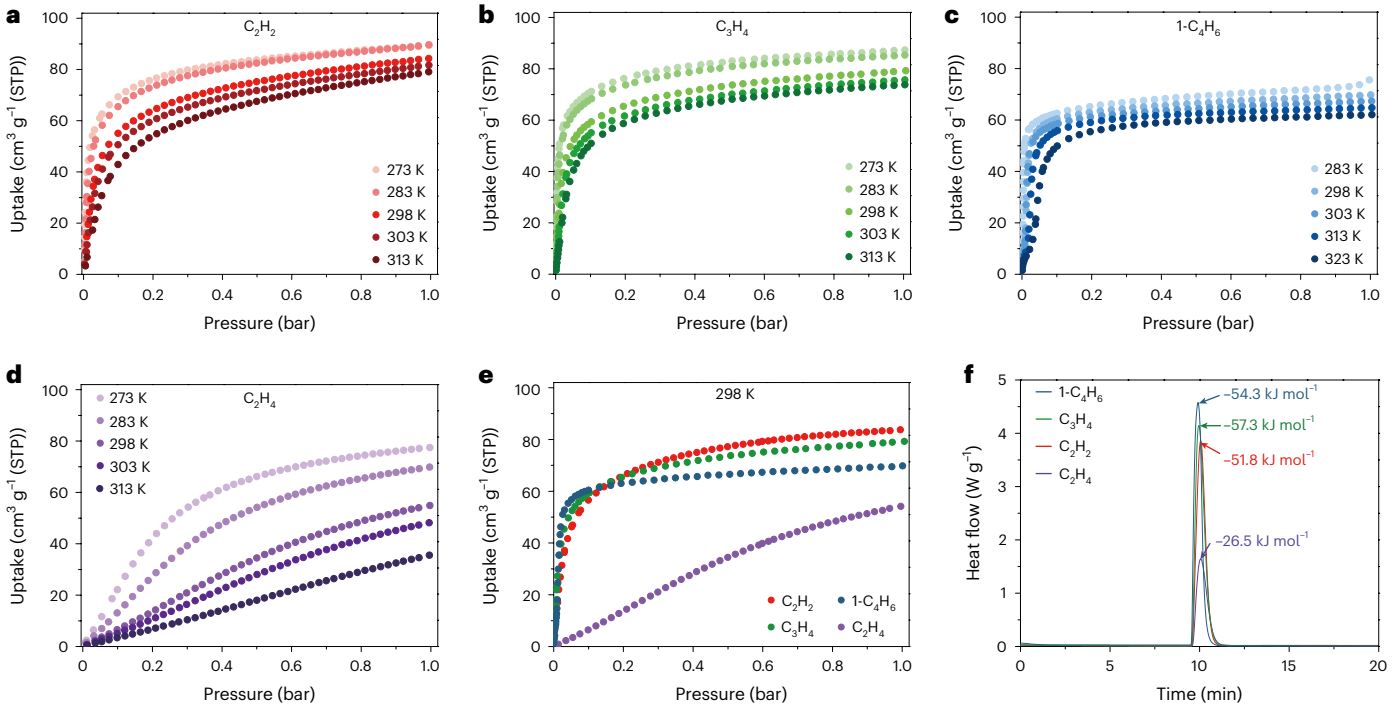

Fig. 2 | Measured equilibrium adsorption and adsorption enthalpy. a–d, Adsorption isotherms of JNU-3a at different temperatures for C_2H_2 (**a**), C_3H_4 (**b**), 1-C_4H_6 (**c**) and C_2H_4 (**d**), (STP, standard temperature and pressure, 273.15 K and 101.325 kPa). **e**, Comparison of C_2H_2 (red), C_3H_4 (green), 1-C_4H_6 (blue) and C_2H_4 (purple) adsorption isotherms of JNU-3a at 298 K. **f**, Differential scanning calorimetry curves upon introducing C_2H_2 (red), C_3H_4 (green), 1-C_4H_6 (blue) and C_2H_4 (purple) on JNU-3a at 298 K and 1 bar.

Gas adsorption

Single-component adsorption isotherms of C_2H_2, C_2H_4, C_3H_4 and 1-C_4H_6 on JNU-3a were collected at various temperatures. As shown in Fig. 2a–c, all three alkynes exhibit steep slopes at low pressures, indicating effective adsorption and a strong binding affinity, whereas C_2H_4 exhibits a gentle slope over the entire pressure range (Fig. 2d), indicating a weaker binding affinity and less effective adsorption. The difference is rather obvious if we compare their adsorption isotherms at 298 K (Fig. 2e). It is worth noting that the C_2H_4 adsorption capacity drops substantially with increasing temperature. For example, at 283 K and 1 bar, the adsorption capacity for C_2H_4 is 69.9 cm^3 g^{-1}, which is slightly lower than those for C_2H_2, C_3H_4 and 1-C_4H_6 (89.7, 85.4 and 75.6 cm^3 g^{-1}, respectively), whereas at 333 K and 1 bar the adsorption capacity for C_2H_4 is 16.4 cm^3 g^{-1}, which is about four times lower than that for C_2H_2, C_3H_4 and 1-C_4H_6 (67.8, 64.0 and 59.2 cm^3 g^{-1}, respectively). The stark contrast in adsorption between the alkynes and C_2H_4 suggests an interesting prospect of JNU-3a for concurrently removing alkynes (C_2H_2 + C_3H_4 + 1-C_4H_6) from C_2H_4 regardless of their molecular sizes.

Adsorption enthalpy and selectivity

To quantify the binding affinity for these hydrocarbons on JNU-3a, the isosteric heat of adsorption (Q_{st}) was calculated using a virial equation derived from the fitting of their adsorption isotherms at three different temperatures (Supplementary Figs. 5–9). The calculated Q_{st} values for C_2H_2, C_3H_4 and 1-C_4H_6 on JNU-3a at low coverage were 33.9, 47.7 and 39.8 kJ mol^{-1}, respectively. Although they are higher than that for C_2H_4 (31.7 kJ mol^{-1}) (Supplementary Fig. 9), these values do not seem to justify the compelling difference in their adsorption isotherms (Fig. 2e). To quantify the isosteric heat of adsorption experimentally, we performed differential scanning calorimetry measurements of heat release upon introducing C_2H_2, C_2H_4, C_3H_4 or 1-C_4H_6 over JNU-3a at 298 K and 1 bar (Fig. 2f). As expected, the experimental Q_{st} values for C_2H_2, C_3H_4 and 1-C_4H_6 (51.8, 57.3 and 54.3 kJ mol^{-1}, respectively) are about twice that for C_2H_4 (26.5 kJ mol^{-1}), confirming the rather preferential adsorption of the three alkynes over C_2H_4, as reflected by their adsorption isotherms. One may argue that the relatively large Q_{st} values for the three alkynes lead to issues during the regeneration of JNU-3a. Hence, we carried out continuous gas adsorption/desorption measurements for C_2H_2, C_2H_4, C_3H_4 and 1-C_4H_6 at 298 K without applying heat at the degassing stage; no obvious losses in adsorption capacity were observed after multiple adsorption/desorption cycles for C_2H_2, C_2H_4, C_3H_4 and 1-C_4H_6 (Supplementary Figs. 10–13). The results not only demonstrate the recyclability of JNU-3a but also suggest the potential for energy-efficient regeneration during the adsorptive separation of these hydrocarbons.

Ideal adsorbed solution theory (IAST)[31] is one of the most used methods for predicting the adsorption behavior of binary gas mixtures based on their single-component adsorption isotherms. To illustrate the preferential adsorption of the three alkynes from their respective mixtures with C_2H_4, IAST was applied to quantitatively estimate the adsorption selectivity for mixtures of C_2H_2/C_2H_4 (1:99), C_3H_4/C_2H_4 (1:99) and 1-C_4H_6/C_2H_4 (1:99) (Supplementary Figs. 16–22 and Supplementary Table 4). For C_2H_2/C_2H_4 (1:99), the IAST adsorption selectivity on JNU-3a was calculated to be 120. Although lower than the C_2H_2/C_2H_4 adsorption selectivity values of benchmark materials such as UTSA-200 (adsorption selectivity 6,320)[26], ZU-33 (>1,000)[32] NCU-100 (7,291)[21] and NKMOF-1-Ni (1,272.6)[33], this value is comparable to or higher than other top-performing materials such as ZUL-100 (175)[22], $Ni_3(pzdc)_2(7Hade)_2$ (168)[34], SIFSIX-2-Cu-i (44)[5], UTSA-100 (10)[35], M′MOF-3a (24)[36], MUF-17 (7)[37] and Fe-MOF-74 (2)[10]. For C_3H_4/C_2H_4 (1:99) and 1-C_4H_6/C_2H_4 (1:99), the IAST adsorption selectivity on JNU-3a was calculated to be 261 and 632, respectively, and these values are substantially higher than contrast MOFs (SIFSIX-2-Cu-i, SIFSIX-3-Ni, ELM-12, CoMOF-74, HKUST-1 and ZJU-74) (Supplementary Figs. 23–28 and Supplementary Table 5). The excellent adsorption selectivity of all three alkynes over C_2H_4 further corroborates that JNU-3a is a promising candidate for removing trace alkynes (C_2H_2 + C_3H_4 + 1-C_4H_6) from C_2H_4.

https://doi.org/10.1038/s44286-023-00004-2

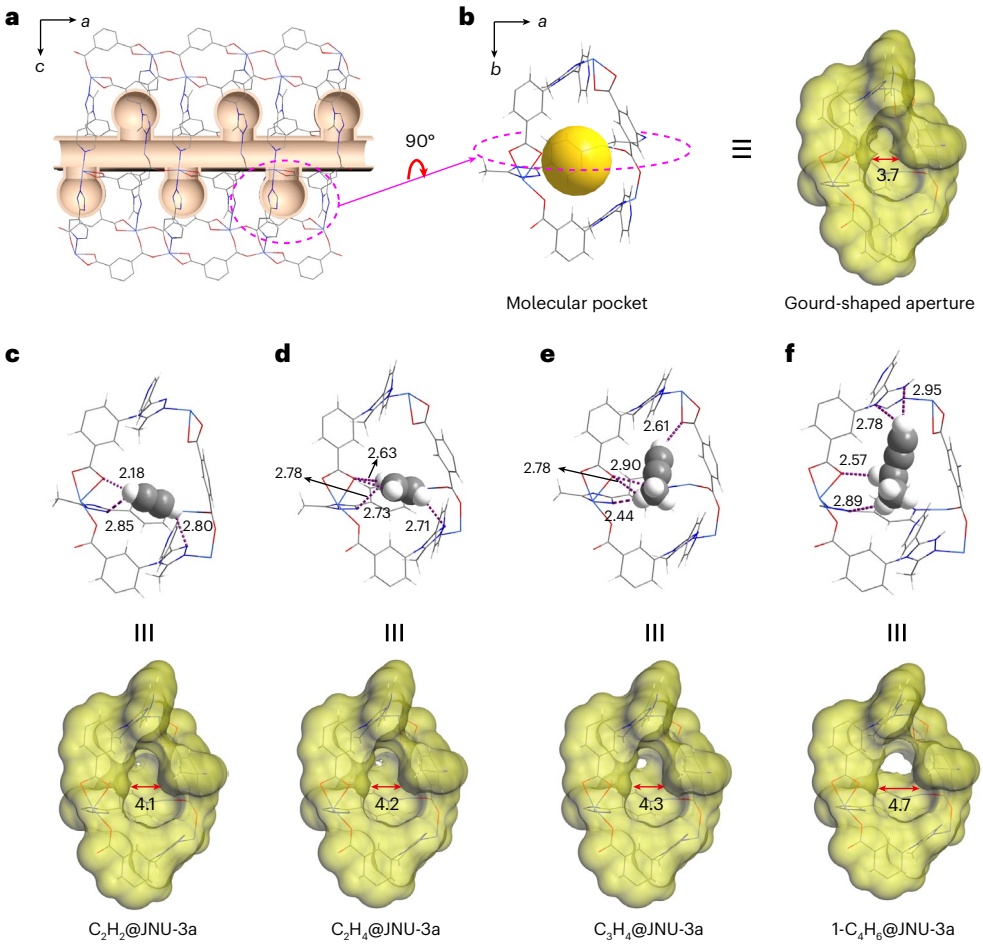

Fig. 3 | Structure and dynamics of the molecular pocket. a, Crystal structure of JNU-3a viewed along the *b* axis with molecular pockets and the 1D channel highlighted. Hydrogen atoms are omitted for clarity. **b**, Molecular pocket viewed along the *c* axis (left) and Connolly surface rendering of the gourd-shaped aperture (right). **c**–**f**, Binding interactions of C_2H_2 (**c**), C_2H_4 (**d**), C_3H_4 (**e**) and 1-C_4H_6 (**f**) inside the molecular pocket according to their individual in situ single-crystal X-ray diffraction data at 150 K (top) and corresponding Connolly surface rendering of the opening up of the gourd-shaped aperture (bottom). Hydrocarbons are depicted in space-filling mode. A probe radius of 0.8 Å was adopted for the Connolly surface calculations. Color code: Co, light blue; O, red; N, dark blue; H, white; C, gray. For **b**–**f**, all distances are given in ångströms.

Gas-loaded crystal structures and computational studies

To gain deeper insight into the host–guest interactions, we performed in situ single-crystal studies for JNU-3a upon loading C_2H_2, C_2H_4, C_3H_4 or 1-C_4H_6 (Supplementary Table 11). Single-crystal X-ray diffraction data for the gas-loaded JNU-3a (termed gas@JNU-3a) were collected at a low temperature (150 K) to minimize the thermal disorder of the adsorbed gas molecules. The crystal structures of C_2H_2@JNU-3a, C_2H_4@JNU-3a, C_3H_4@JNU-3a and 1-C_4H_6@JNU-3a show that all of the hydrocarbons are preferentially adsorbed inside the molecular pockets and that each pocket accommodates one crystallographically unique C_2H_2, C_2H_4, C_3H_4 or 1-C_4H_6 molecule. A closer look at the crystal structures reveals that hydrocarbons exhibit multiple non-classical hydrogen-bonding interactions with the O/N atoms of the surrounding organic linkers on the pocket (Fig. 3c–f). Connolly surface comparison clearly shows the opening of the apertures; the narrowest diameter was increased from 3.7 Å to 4.1, 4.2, 4.3 and 4.7 Å upon loading of C_2H_2, C_2H_4, C_3H_4 and 1-C_4H_6, respectively (Fig. 3b–f). Electrostatic potential maps of C_2H_2, C_2H_4, C_3H_4 and 1-C_4H_6 inside the pocket were rendered using the VMD program (v.1.9.3)[38] based on the outputs of the Multiwfn program[39]. The red and blue surfaces of these maps enable us to visualize the electrostatic potential and strong binding sites (Supplementary Fig. 33). To quantify the interactions of C_2H_2, C_2H_4, C_3H_4 and 1-C_4H_6 inside the pockets, first-principles density functional theory calculations were performed on a cluster model using the Gaussian 16 program[40] (Supplementary Fig. 34). The static binding energy E_b values (Supplementary Methods, Computational details) were calculated to be −49.9, −55.5 and −51.6 kJ mol^{-1} for C_2H_2, C_3H_4 and 1-C_4H_6, respectively, which are substantially higher than that for C_2H_4 (−27.0 kJ mol^{-1}) and consistent with the measured Q_{st} values for the three alkynes and C_2H_4. The results further demonstrate the potential of JNU-3a for splitting C_2H_4 from mixtures with the three alkynes in a single adsorption step.

Laboratory-scale breakthrough experiments

To evaluate the practicality of JNU-3a as an adsorbent for the simultaneous removal of alkynes from C_2H_4 mixtures, laboratory-scale column breakthrough experiments (Supplementary Fig. 35) on 1.4 g of JNU-3a were first performed for a C_2H_2/C_3H_4/1-C_4H_6/C_2H_4 mixture (1:1:1:97) with a flow rate of 4.0 ml min^{-1} at 298 K. As shown in Fig. 4a, an excellent performance for C_2H_4 purification was observed. C_2H_4 quickly broke through the column at 24 min g^{-1}, whereas C_2H_2, 1-C_4H_6 and C_3H_4 were captured and did not break through the column until 252, 254 and 279 min g^{-1}, respectively, indicating negligible competition between them for the molecular pockets. Gas chromatography with flame ionization detection was used to analyse the composition of the eluents, and a 5 ppm cut-off line was delineated in the Fig. 4a inset to highlight the ultrahigh purity of C_2H_4 (>99.9995%) from 24 min g^{-1} to

https://doi.org/10.1038/s44286-023-00004-2

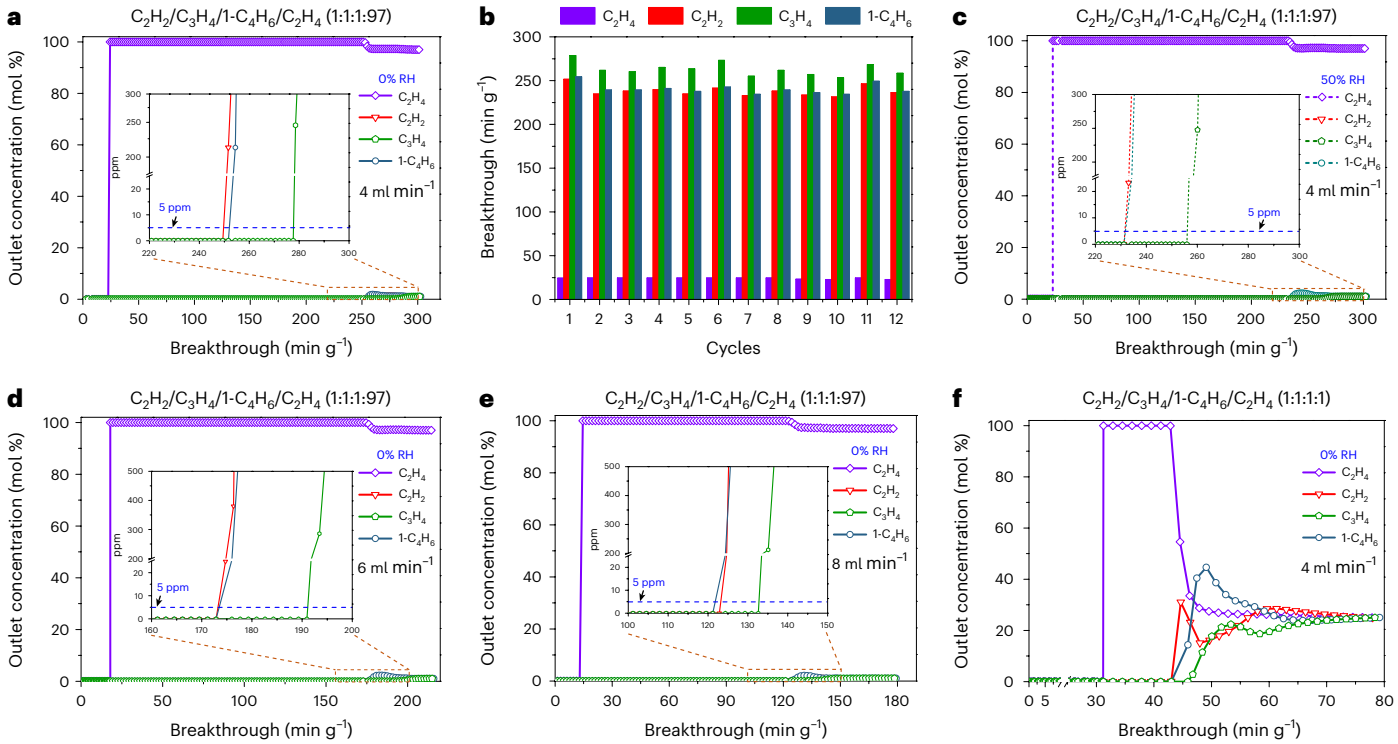

Fig. 4 | Small-scale column breakthrough and recyclability. a, Breakthrough curves for a $C_2H_2/C_3H_4/1\text{-}C_4H_6/C_2H_4$ mixture (1:1:1:97) on 1.4 g of JNU-3a at 298 K (flow rate: 4.0 ml min^{-1}). The inset shows an enlargement of the C_2H_2, C_3H_4 and 1-C_4H_6 concentrations at breakthrough. **b**, Comparison of breakthrough times over 12 cycles of breakthrough experiments on 1.4 g of JNU-3a for a $C_2H_2/C_3H_4/1\text{-}C_4H_6/C_2H_4$ mixture (1:1:1:97) at 298 K (flow rate: 4.0 ml min^{-1}). In situ regeneration was carried out under vacuum at 298 K for 24 h. **c**, Breakthrough curves for a $C_2H_2/C_3H_4/1\text{-}C_4H_6/C_2H_4$ mixture (1:1:1:97) on 1.4 g of JNU-3a at 298 K under humid conditions (50% RH) (flow rate: 4.0 ml min^{-1}). The inset shows an enlargement of the C_2H_2, C_3H_4 and 1-C_4H_6 concentrations at breakthrough. **d**, Breakthrough curves for a $C_2H_2/C_3H_4/1\text{-}C_4H_6/C_2H_4$ mixture (1:1:1:97) on 1.4 g of JNU-3a at 298 K (flow rate: 6.0 ml min^{-1}). The inset shows an enlargement of the C_2H_2, C_3H_4 and 1-C_4H_6 concentrations at breakthrough. **e**, Breakthrough curves for a $C_2H_2/C_3H_4/1\text{-}C_4H_6/C_2H_4$ mixture (1:1:1:97) on 1.4 g of JNU-3a at 298 K (flow rate: 8.0 ml min^{-1}). The inset shows an enlargement of the C_2H_2, C_3H_4 and 1-C_4H_6 concentrations at breakthrough. **f**, Breakthrough curves for a $C_2H_2/C_3H_4/1\text{-}C_4H_6/C_2H_4$ mixture (1:1:1:1) on 1.4 g of JNU-3a at 298 K (flow rate: 4.0 ml min^{-1}).

252 min g^{-1} at the outlet. Continuous breakthrough experiments were performed under the aforementioned conditions and with a vacuum applied at 298 K for 24 h as a regeneration method. As shown in Fig. 4b and Supplementary Figs. 37–40, the breakthrough times for each of the four hydrocarbons fluctuated by just a few minutes at most, indicating that achieving high-purity C_2H_4 was maintained over 12 cycles, further manifesting the durability and recyclability of JNU-3a for one-step C_2H_4 purification from its mixtures with C_2H_2, 1-C_4H_6 and C_3H_4.

The selective adsorption of alkynes over C_2H_4 by MOF materials may not be particularly difficult considering their substantial difference in polarizability and pK_a values. However, the simultaneous removal of C_4H_6, C_3H_4 and C_2H_2 from C_2H_4 by MOF materials is fundamentally challenging due to the competition of the three alkynes for the adsorption sites. In JNU-3a, the three alkynes exhibit negligible competition for the molecular pockets. To experimentally support this hypothesis, six MOFs (SIFSIX-2-Cu-i, SIFSIX-3-Ni, ELM-12, CoMOF-74, HKUST-1 and ZJU-74) were selected as contrast materials. We first measured their single-component adsorption for C_2H_2, C_2H_4, C_3H_4 and 1-C_4H_6 at 298 K. The data are consistent with literature reports[5,24,25,41–43]. We then carried out repeated column breakthrough experiments for a $C_2H_2/C_3H_4/1\text{-}C_4H_6/C_2H_4$ mixture (1:1:1:97) under similar conditions. As shown in Extended Data Figs. 1 and 2, for the six contrast MOFs, at least one alkyne breaks through the column at a very early time, indicating substantial competition between the three alkynes for the adsorption sites. On the basis of the breakthrough curves, 841.4 ml g^{-1} of high-purity C_2H_4 (≥99.9995%) was estimated to be collectable in a single breakthrough operation for JNU-3a; this value is nearly 15-fold that for SIFSIX-3-Ni (58.2 ml g^{-1}) and ZJU-74 (52.5 ml g^{-1}), 17-fold that for ELM-12 (47.8 ml g^{-1}) and more than 100-fold that for CoMOF-74 (7.8 ml g^{-1}) (Extended Data Table 1). Furthermore, we carried out breakthrough experiments with varying C_2H_2/C_3H_4 ratios at a fixed total ratio of alkyne ($C_2H_2 + C_3H_4$) to alkene (C_2H_4) on JNU-3a and CoMOF-74 (Supplementary Tables 8 and 9 and Supplementary Figs. 43 and 44). For JNU-3a, data analyses show that the breakthrough times for both C_2H_2 and C_3H_4 are largely independent of their ratios in the feed gas and that the C_2H_2/C_3H_4 values captured in the breakthrough column are close to their ratios in the feed gas; however, for the contrast MOF (CoMOF-74), the C_2H_2/C_3H_4 values captured in the breakthrough column are vastly different from their ratios in the feed gas (Extended Data Fig. 3). For ideal non-competitive adsorption, C_2H_2 and C_3H_4 should break through the column at the same time, regardless of their ratios in the feed gas, and the C_2H_2/C_3H_4 values captured in the breakthrough column should be consistent with their ratios in the feed gas. The contrast breakthrough experiments support the proposed non-competitive adsorption of alkynes in JNU-3a.

Industrial crude C_2H_4 often contains trace amounts of water vapor[4]. To investigate the influence of moisture on the high-purity C_2H_4 produced, we performed column breakthrough experiments for a $C_2H_2/C_3H_4/1\text{-}C_4H_6/C_2H_4$ mixture (1:1:1:97) at a relative humidity (RH) of 50%. As shown in Fig. 4c, the breakthrough times for the four hydrocarbons were relatively unchanged, and a high-purity C_2H_4 productivity of 814.6 ml g^{-1} was estimated, which is slightly lower than that under dry conditions of zero RH (841.4 ml g^{-1}) (Extended Data Table 2). We also performed continuous breakthrough experiments under the aforementioned conditions and with a vacuum applied at 298 K for

https://doi.org/10.1038/s44286-023-00004-2

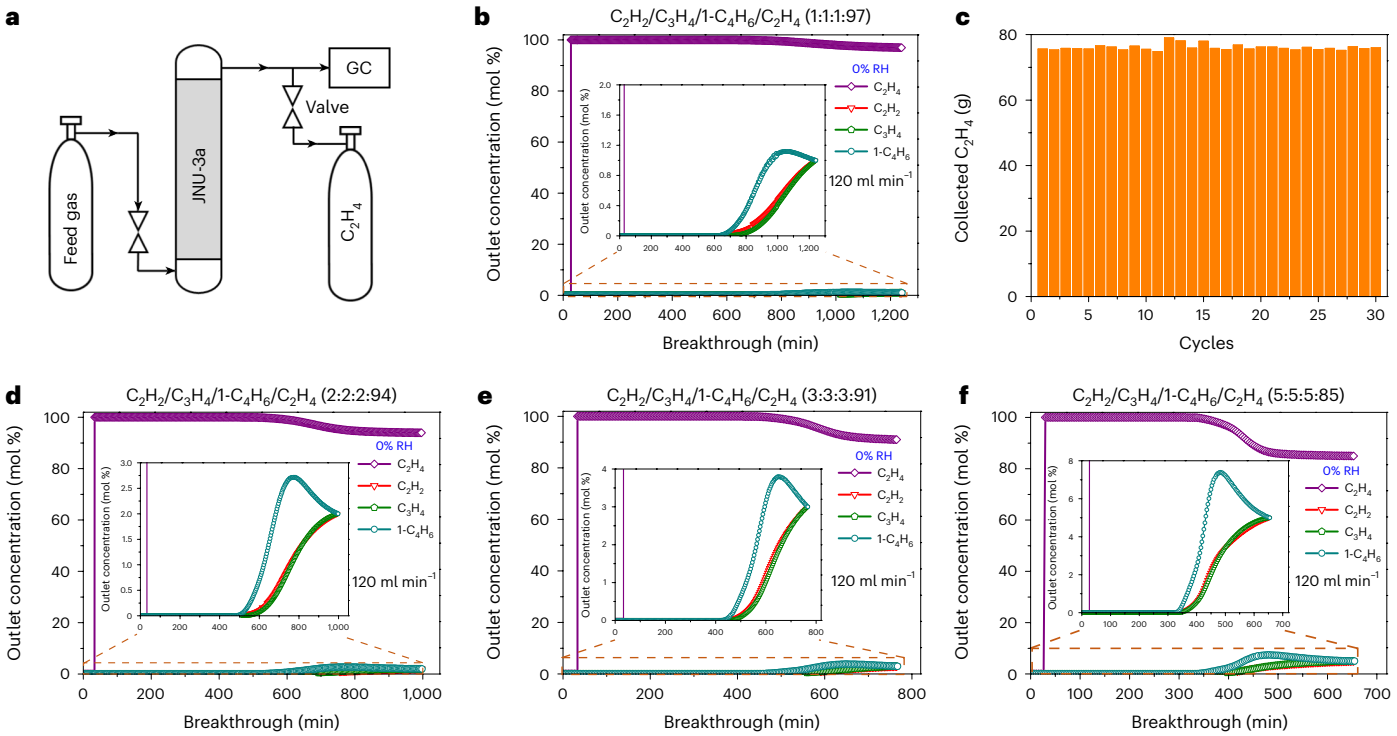

Fig. 5 | Pilot-scale column breakthrough and gas-cylinder C_2H_4 collection. **a**, Simplified representation of the pilot-scale column breakthrough setup with a gas cylinder for outgas collection. GC, gas chromatography. **b**, Breakthrough curves for a $C_2H_2/C_3H_4/1\text{-}C_4H_6/C_2H_4$ mixture (1:1:1:97) on 107 g of JNU-3a. The inset shows the breakthrough times and relative concentrations of C_2H_2, C_3H_4, $1\text{-}C_4H_6$ and C_2H_4. **c**, Summary of the amount of C_2H_4 collected over 30 cycles of column breakthrough on JNU-3a (107 g) for a $C_2H_2/C_3H_4/1\text{-}C_4H_6/C_2H_4$ mixture (1:1:1:97). **d**–**f**, Breakthrough curves on 107 g of JNU-3a for $C_2H_2/C_3H_4/1\text{-}C_4H_6/C_2H_4$ mixtures with respective component ratios of 2:2:2:94 (**d**), 3:3:3:91 (**e**) and 5:5:5:85 (**f**). The inset for each shows the breakthrough times and relative concentrations of C_2H_2, C_3H_4, $1\text{-}C_4H_6$ and C_2H_4.

24 h as a regeneration method. Almost the same breakthrough times were observed for C_2H_2, $1\text{-}C_4H_6$, C_3H_4 and C_2H_4, indicating no loss in C_2H_4 productivity after three cycles of breakthrough experiments under humid conditions (Supplementary Fig. 48). The results suggest a low impact of moisture on the purification of C_2H_4 from its mixture with C_2H_2, C_3H_4 and $1\text{-}C_4H_6$.

To investigate the influence of the flow rate on the productivity of high-purity C_2H_4, we performed column breakthrough experiments for a $C_2H_2/C_3H_4/1\text{-}C_4H_6/C_2H_4$ mixture (1:1:1:97) at different flow rates (of up to 8.0 ml min^{-1}) (Fig. 4d,e and Supplementary Fig. 49). The breakthrough times of all four hydrocarbons were reduced with an increase in the flow rate, yet the productivity of high-purity C_2H_4 was retained: values of 782.9, 912.8 and 854.7 ml g^{-1} were obtained at flow rates of 2.0, 6.0 and 8.0 ml min^{-1}, respectively (Extended Data Table 2). Next, we performed column breakthrough experiments for a $C_2H_2/C_3H_4/1\text{-}C_4H_6/C_2H_4$ mixture (1:1:1:1) at a flow rate of 4.0 ml min^{-1} (Fig. 4f). To our surprise, high-purity C_2H_4 (>99.9995%) can still be realized at the outlet for a substantial period of time, and the productivity was estimated to be 9.9 ml g^{-1}. We also performed continuous breakthrough experiments under the aforementioned conditions an with a vacuum applied at 298 K for 24 h as a regeneration method (Supplementary Fig. 50). Almost the same breakthrough times were observed for C_2H_4, C_2H_2, C_3H_4 and $1\text{-}C_4H_6$, indicating no loss of C_2H_4 productivity after three cycles of breakthrough experiments for the 1:1:1:1 mixture. The results further demonstrate the excellent separation capability of high-purity C_2H_4 from its mixture with C_2H_2, C_3H_4 and $1\text{-}C_4H_6$.

Pilot-scale breakthrough experiments

Current laboratory-scale column breakthrough experiments are usually run on a small amount of adsorbent (~1.0 g), and the reported productivity is estimated from the breakthrough curves and not by actual outgas collection. For potential industrial development, a laboratory-sized pilot-scale column breakthrough experiment on 107 g of JNU-3a was set up with a gas cylinder (of eight liter capacity) for outgas collection (Fig. 5a, Extended Data Fig. 4 and Supplementary Figs. 51–53). We demonstrated the collection of high-purity C_2H_4 (≥99.9995%) from $C_2H_2/C_3H_4/1\text{-}C_4H_6/C_2H_4$ mixtures of different ratios in a single adsorption step at room temperature (Fig. 5b,d–f and Extended Data Table 3). The amount and purity of the collected C_2H_4 in the gas cylinder were determined via weight measurement and gas chromatography, respectively. In particular, an average of 76.1 ± 1.3 g of high-purity C_2H_4 was obtained from a $C_2H_2/C_3H_4/1\text{-}C_4H_6/C_2H_4$ mixture (1:1:1:97) at a flow rate of 120 ml min^{-1} over 30 cycles (Fig. 5c and Extended Data Table 4), which is equivalent to a productivity of 569 ml g^{-1} (C_2H_4/JNU-3a) under standard conditions.

Outlook

Given their potential of recognizing guest molecules through host–guest interactions, MOFs with local flexibility may offer an unorthodox separation capability for a multicomponent mixture regardless of the molecular sizes of the components. In this work we present a robust MOF material (JNU-3a) for the direct production of high-purity C_2H_4 (≥99.9995%) from $C_2H_2/C_3H_4/1\text{-}C_4H_6/C_2H_4$ mixtures in a single adsorption step. Combined characterization techniques and theoretical calculations reveal that the dynamic molecular pockets on both sides of the 1D channel preferentially open to the three alkynes, resulting in an excellent separation capacity for high-purity C_2H_4 from $C_2H_2/C_3H_4/1\text{-}C_4H_6/C_2H_4$ mixtures. As a proof of concept, we demonstrate pilot-scale breakthrough and gas-cylinder C_2H_4 collection on 107 g of JNU-3a for $C_2H_2/C_3H_4/1\text{-}C_4H_6/C_2H_4$ mixtures of different ratios. JNU-3a maintains its

separation potential, affording an average of 76.1 g of high-purity C_2H_4 per cycle over 30 cycles for a $C_2H_2/C_3H_4/1\text{-}C_4H_6/C_2H_4$ mixture (1:1:1:97). Overall, the underlying channel-pocket structure of JNU-3a makes it ideal for concurrently removing C_2–C_4 alkynes from C_2H_4 mixtures with high efficiency. We envision that further engineering on the molecular pocket will enable the application-oriented regulation of host–guest interactions to cater to diverse industrial needs. As the large-scale synthesis technology of MOFs continues to advance, the environmental and energetic benefits of applying MOF adsorbents for gas separation and purification will eventually outweigh the initial investment.

Methods

Materials

All reagents and solvents were obtained commercially and used as received without further purification. The ligand 5-(3-methyl-5-(pyridin-4-yl)-4*H*-1,2,4-triazol-4-yl)-1,3-benzenedicarboxylic acid was purchased from Shanghai Tensus Biotech Company. Ultrahigh-purity grades of Ar (>99.999%), C_2H_2 (>99%), C_2H_4 (>99.99%), C_3H_4 (>99%) and $1\text{-}C_4H_6$ (>99.7%) were purchased from Dalian Special Gases. $C_2H_2/C_3H_4/C_2H_4$ and $C_2H_2/C_3H_4/1\text{-}C_4H_6/C_2H_4$ mixed gases were purchased from Guangdong Huate Gas Company.

Preparation of JNU-3

JNU-3 was prepared according to a previously reported method[30]. JNU-3a (the activated JNU-3) was obtained under vacuum (<5 μm Hg) at 150 °C for 24 h.

Gas adsorption measurements

JNU-3a (≥100 mg) was used for each measurement. Further degassing and single-component adsorption/desorption procedures at different temperatures were conducted using a Micromeritics ASAP 2020 PLUS analyser.

Single-crystal X-ray diffraction analysis

Gas-loaded JNU-3a was prepared by exposing the JNU-3a crystal structure to a gas atmosphere of 1 bar at room temperature for 1 h. Single-crystal diffraction data for C_2H_2@JNU-3a, C_2H_4@JNU-3a, C_3H_4@JNU-3a and $1\text{-}C_4H_6$@JNU-3a were collected at 150 K using an Oxford Cryo stream system on an XtaLAB PRO MM007-DW diffractometer system equipped with an RA-Micro7HF-MR-DW (Cu/Mo) X-ray generator and HyPix-6000HE hybrid photon counting X-ray detector (Rigaku; Cu Kα, λ = 1.5418 Å). The structures were solved and refined using the Olex2 program with the 'XS' and 'XL' plugins[44].

Regeneration methods for column breakthrough

For laboratory-scale (1.4 g of JNU-3a) column breakthrough experiments, the sample was regenerated in situ in the column by applying a vacuum (using a turbo molecular pump) at 298 K for 24 h. For the pilot-scale (107 g of JNU-3a) column breakthrough experiments, the sample was regenerated in situ in the column under vacuum (turbo molecular pump) at 333 K for 12 h.

Data availability

All data supporting the findings of this study are available within the paper and its supplementary materials. Crystallographic data for the structures reported in this Article have been deposited at the Cambridge Crystallographic Data Centre, under deposition numbers CCDC 2093003 (C_2H_2@JNU-3a), 2093004 (C_2H_4@JNU-3a), 2120227 ($1\text{-}C_4H_6$@JNU-3a) and 2120228 (C_3H_4@JNU-3a). Copies of the data can be obtained free of charge via https://www.ccdc.cam.ac.uk/structures/. Source data are provided with the paper.

References

1. Matar, S. & Hatch, L. F. *Chemistry of Petrochemical Processes* 2nd edn (Gulf Professional Publishing, 2001).
2. Li, L. et al. Ethane/ethylene separation in a metal–organic framework with iron-peroxo sites. *Science* **362**, 443–446 (2018).
3. *Ethylene (ET): 2023 World Market Outlook up to 2032* (Merchant Research and Consulting Ltd, 2023); https://www.researchandmarkets.com/research/5rkr9b/world_ethylene?w=12.
4. Zimmermann, H. & Walzl, R. Ethylene. In *Ullmann's Encyclopedia of Industrial Chemistry 7th edn* 465–529 (John Wiley & Sons, Ltd, 2009).
5. Cui, X. et al. Pore chemistry and size control in hybrid porous materials for acetylene capture from ethylene. *Science* **353**, 141–144 (2016).
6. Buschbeck, R., Low, P. J. & Lang, H. Homoleptic transition metal acetylides. *Coord. Chem. Rev.* **255**, 241–272 (2011).
7. Molero, H., Bartlett, B. F. & Tysoe, W. T. The hydrogenation of acetylene catalyzed by palladium: hydrogen pressure dependence. *J. Catal.* **181**, 49–56 (1999).
8. Teschner, D. et al. The roles of subsurface carbon and hydrogen in palladium-catalyzed alkyne hydrogenation. *Science* **320**, 86–89 (2008).
9. Chen, K.-J. et al. Synergistic sorbent separation for one-step ethylene purification from a four-component mixture. *Science* **366**, 241–246 (2019).
10. Bloch, E. D. et al. Hydrocarbon separations in a metal–organic framework with open iron(II) coordination sites. *Science* **335**, 1606–1610 (2012).
11. Ji, Z. et al. Sequencing of metals in multivariate metal–organic frameworks. *Science* **369**, 674–680 (2020).
12. Zhou, H. C., Long, J. R. & Yaghi, O. M. Introduction to metal–organic frameworks. *Chem. Rev.* **112**, 673–674 (2012).
13. Zhou, H. C. & Kitagawa, S. Metal–organic frameworks (MOFs). *Chem. Soc. Rev.* **43**, 5415–5418 (2014).
14. Zhao, X. et al. Metal–organic frameworks for separation. *Adv. Mater.* **30**, 1705189 (2018).
15. Yaghi, O. M., Kalmutzki, M. J. & Diercks, C. S. *Introduction to Reticular Chemistry: Metal–Organic Frameworks and Covalent Organic Frameworks* (Wiley, 2019).
16. Kirchon, A. et al. From fundamentals to applications: a toolbox for robust and multifunctional MOF materials. *Chem. Soc. Rev.* **47**, 8611–8638 (2018).
17. Chen, B., Xiang, S. C. & Qian, G. D. Metal–organic frameworks with functional pores for recognition of small molecules. *Acc. Chem. Res.* **43**, 1115–1124 (2010).
18. Yang, L. et al. Energy-efficient separation alternatives: metal–organic frameworks and membranes for hydrocarbon separation. *Chem. Soc. Rev.* **49**, 5359–5406 (2020).
19. Wang, H. et al. Designer metal–organic frameworks for size-exclusion-based hydrocarbon separations: progress and challenges. *Adv. Mater.* **32**, 2002603 (2020).
20. Li, J. et al. Recent progress on microfine design of metal–organic frameworks: structure regulation and gas sorption and separation. *Adv. Mater.* **32**, 2002563 (2020).
21. Wang, J. et al. Optimizing pore space for flexible-robust metal–organic framework to boost trace acetylene removal. *J. Am. Chem. Soc.* **142**, 9744–9751 (2020).
22. Shen, J. et al. Simultaneous interlayer and intralayer space control in two-dimensional metal–organic frameworks for acetylene/ethylene separation. *Nat. Commun.* **11**, 6259 (2020).
23. Chai, Y. et al. Control of zeolite pore interior for chemoselective alkyne/olefin separations. *Science* **368**, 1002–1006 (2020).
24. Pei, J. et al. A chemically stable Hofmann-type metal–organic framework with sandwich-like binding sites for benchmark acetylene capture. *Adv. Mater.* **32**, 1908275 (2020).
25. Li, L. et al. A metal–organic framework with suitable pore size and specific functional sites for the removal of trace propyne from propylene. *Angew. Chem. Int. Ed.* **57**, 15183–15188 (2018).

26. Li, B. et al. An ideal molecular sieve for acetylene removal from ethylene with record selectivity and productivity. *Adv. Mater.* **29**, 1704210 (2017).
27. Lin, R.-B. et al. Optimized separation of acetylene from carbon dioxide and ethylene in a microporous material. *J. Am. Chem. Soc.* **139**, 8022–8028 (2017).
28. Dong, Q. et al. Tuning gate-opening of a flexible metal–organic framework for ternary gas sieving separation. *Angew. Chem. Int. Ed.* **59**, 22756–22762 (2020).
29. Zhou, D. et al. Intermediate-sized molecular sieving of styrene from larger and smaller analogues. *Nat. Mater.* **18**, 994–998 (2019).
30. Zeng, H. et al. Orthogonal-array dynamic molecular sieving of propylene/propane mixtures. *Nature* **595**, 542–548 (2021).
31. Myers, A. L. & Prausnitz, J. M. Thermodynamics of mixed-gas adsorption. *AIChE J.* **11**, 121–127 (1965).
32. Zhang, Z. et al. Hexafluorogermanate (GeFSIX) anion-functionalized hybrid ultramicroporous materials for efficiently trapping acetylene from ethylene. *Ind. Eng. Chem. Res.* **57**, 7266–7274 (2018).
33. Peng, Y. L. et al. Robust ultramicroporous metal–organic frameworks with benchmark affinity for acetylene. *Angew. Chem. Int. Ed.* **57**, 10971–10975 (2018).
34. Zhang, Z. Q. et al. Efficient trapping of trace acetylene from ethylene in an ultramicroporous metal–organic framework: synergistic effect of high-density open metal and electronegative sites. *Angew. Chem. Int. Ed.* **59**, 18927–18932 (2020).
35. Hu, T. L. et al. Microporous metal–organic framework with dual functionalities for highly efficient removal of acetylene from ethylene/acetylene mixtures. *Nat. Commun.* **6**, 7328 (2015).
36. Xiang, S. C. et al. Rationally tuned micropores within enantiopure metal–organic frameworks for highly selective separation of acetylene and ethylene. *Nat. Commun.* **2**, 204 (2011).
37. Qazvini, O. T., Babarao, R. & Telfer, S. G. Multipurpose metal–organic framework for the adsorption of acetylene: ethylene purification and carbon dioxide removal. *Chem. Mater.* **31**, 4919–4926 (2019).
38. Humphrey, W., Dalke, A. & Schulten, K. VMD: visual molecular dynamics. *J. Mol. Graph.* **14**, 33–38 (1996).
39. Lu, T. & Chen, F. W. Multiwfn: a multifunctional wavefunction analyzer. *J. Comput. Chem.* **33**, 580–592 (2012).
40. Frisch, M. J. et al. Gaussian16, revision B.01 (Gaussian Inc., 2016).
41. Li, L. et al. Flexible–robust metal–organic framework for efficient removal of propyne from propylene. *J. Am. Chem. Soc.* **139**, 7733–7736 (2017).
42. Xiang, S. et al. Open metal sites within isostructural metal–organic frameworks for differential recognition of acetylene and extraordinarily high acetylene storage capacity at room temperature. *Angew. Chem. Int. Ed.* **49**, 4615–4618 (2010).
43. Xiang, S. et al. Exceptionally high acetylene uptake in a microporous metal–organic framework with open metal sites. *J. Am. Chem. Soc.* **131**, 12415–12419 (2009).
44. Sheldrick, G. M. SHELXT-Integrated space-group and crystal-structure determination. *Acta Crystallogr. A* **71**, 3–8 (2015).

Acknowledgements

We thank Dr X. Zhen from Minnan Normal University for their advice on computational studies. This work was supported financially by the National Natural Science Foundation of China (numbers 21731002 (D.L.), 21975104 (D.L.), 22150004 (D.L.), 22301102 (H.Z.) and 22271120 (W.L.)), the Guangdong Basic and Applied Basic Research Foundation (number 2023A1515010952 (H.Z.)) and the Project funded by China Postdoctoral Science Foundation (numbers BX20220132 and 2023M741375 (H.Z.)).

Author contributions

W.L. and D.L. conceived and designed the research. X.-J.X. and T.W. synthesized the compounds. H.Z. collected and analysed the gas adsorption and separation data. H.Z. collected the X-ray diffraction data. R.-J.W. analysed the X-ray diffraction data. M.X. and Y.W. performed the theoretical calculations. H.Z., W.L. and D.L. prepared the manuscript. All authors participated in and contributed to the final version.

Competing interests

The authors declare no competing interests.

Additional information

Extended data is available for this paper at https://doi.org/10.1038/s44286-023-00004-2.

Supplementary information The online version contains supplementary material available at https://doi.org/10.1038/s44286-023-00004-2.

Correspondence and requests for materials should be addressed to Weigang Lu or Dan Li.

Peer review information *Nature Chemical Engineering* thanks Banglin Chen, Meihong Wang and the other, anonymous, reviewer(s) for their contribution to the peer review of this work.

https://doi.org/10.1038/s44286-023-00004-2

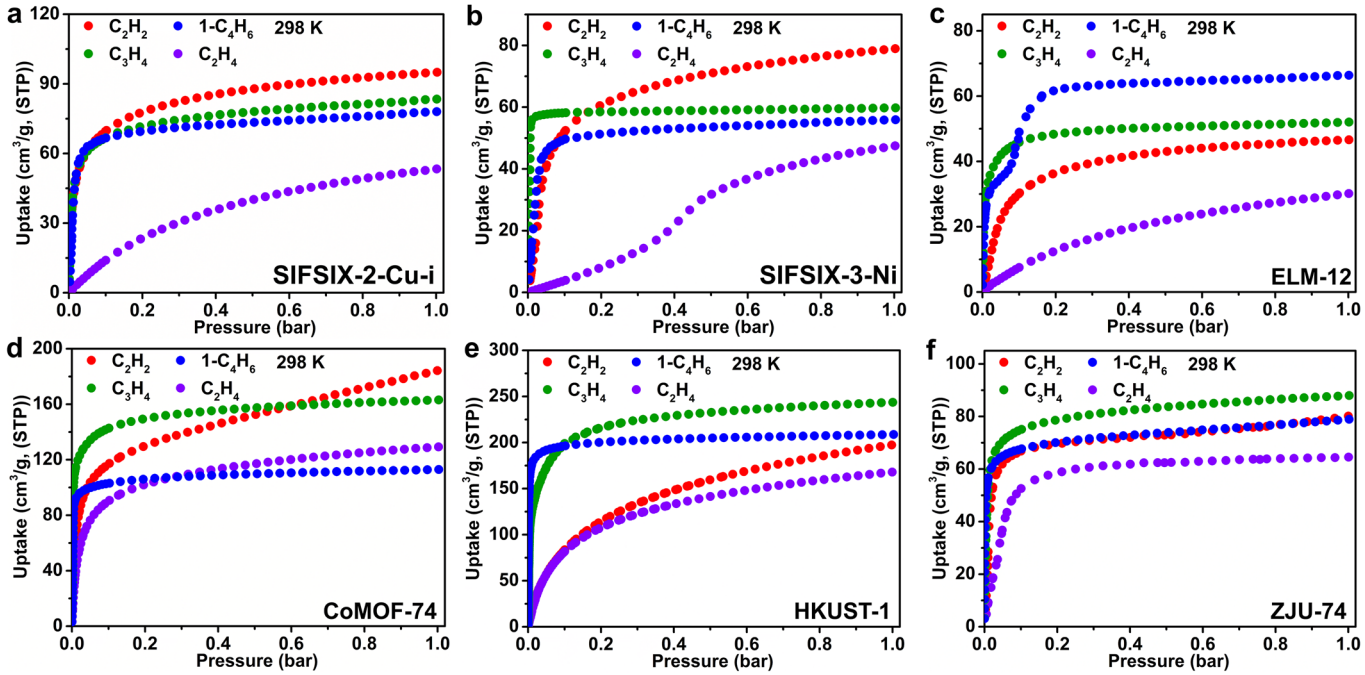

Extended Data Fig. 1 | Measured equilibrium adsorption of contrast MOFs. Single-component adsorption for C_2H_2 (red), C_3H_4 (olive), 1-C_4H_6 (blue), and C_2H_4 (violet) on (**a**) SIFSIX-2-Cu-i, (**b**) SIFSIX-3-Ni, (**c**) ELM-12, (**d**) CoMOF-74, (**e**) HKUST-1, and (**f**) ZJU-74 at 298 K.

https://doi.org/10.1038/s44286-023-00004-2

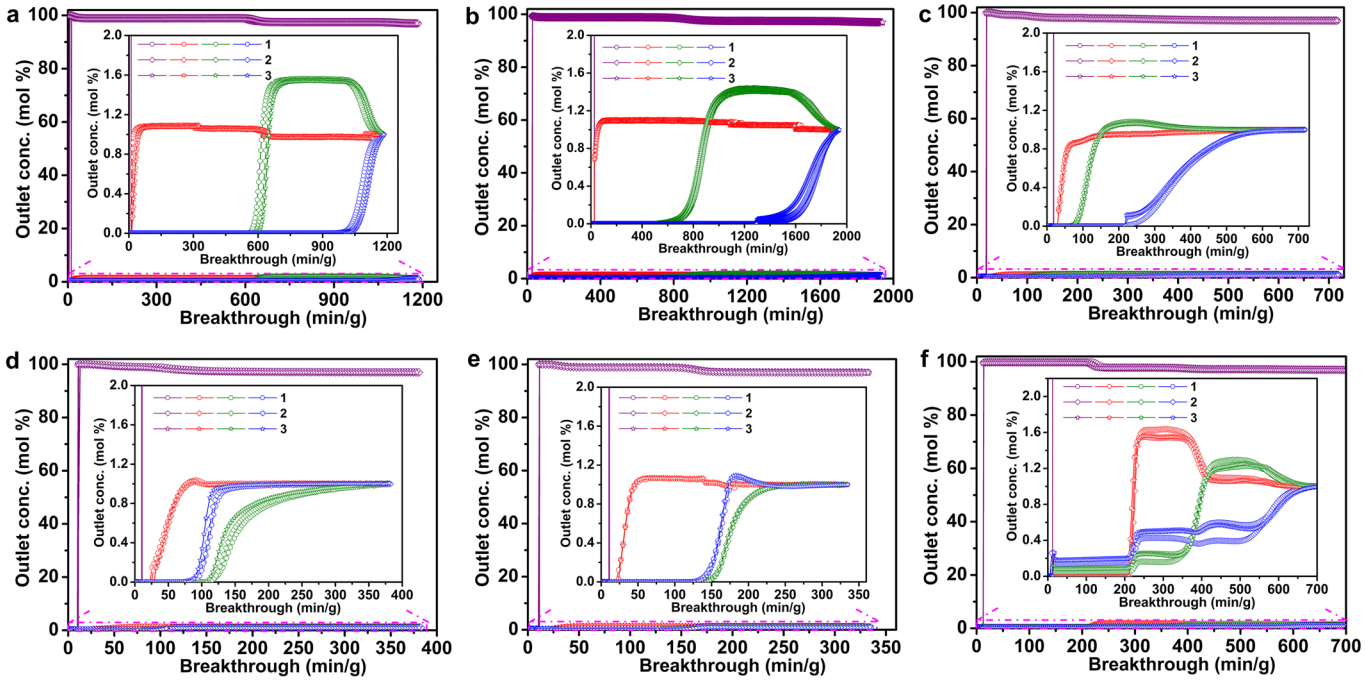

Extended Data Fig. 2 | Column breakthrough and recyclability of contrast MOFs. Three cycles of breakthrough curves for a $C_2H_2/C_3H_4/1\text{-}C_4H_6/C_2H_4$ (1:1:1:97) mixture on (**a**) CoMOF-74, (**b**) HKUST-1, (**c**) ZJU-74, (**d**) SIFSIX-3-Ni, (**e**) ELM-12, and (**f**) SIFSIX-2-Cu-i at 298 K (flow rate: 4.0 mL min^{-1}). The insets show breakthrough times and relative concentrations of C_2H_2, C_3H_4, $1\text{-}C_4H_6$, and C_2H_4.

https://doi.org/10.1038/s44286-023-00004-2

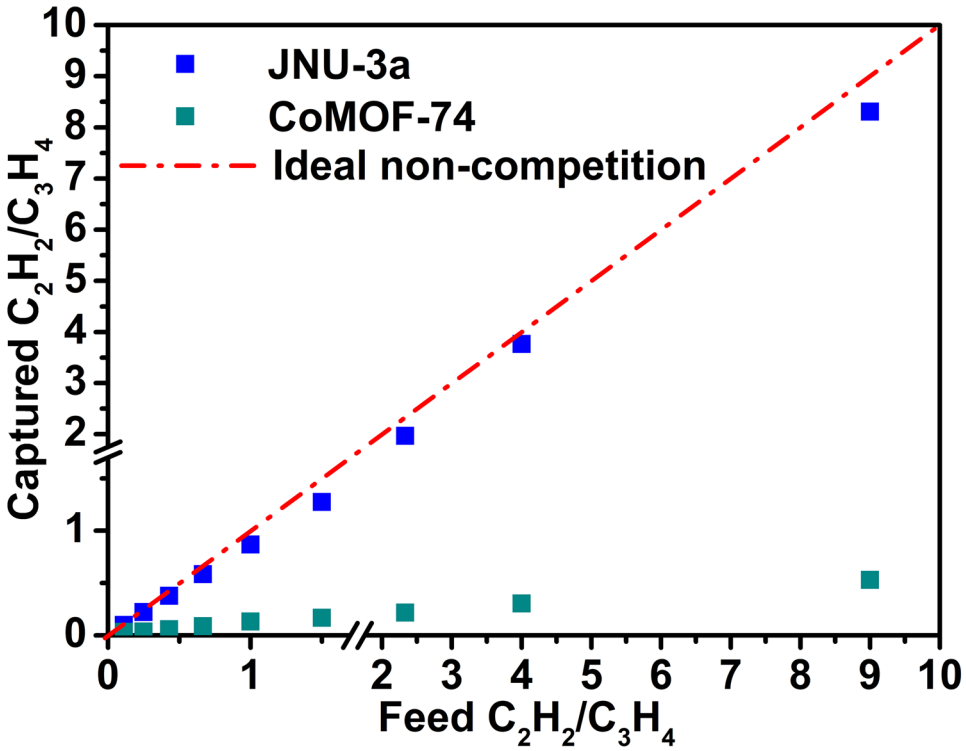

Extended Data Fig. 3 | Non-competitive and competitive adsorption of alkynes. Plots of C_2H_2/C_3H_4 in feed gas against C_2H_2/C_3H_4 captured in breakthrough column for $C_2H_2/C_3H_4/C_2H_4$ mixtures of different ratios (flow rate: 4.0 mL min^{-1}) on JNU-3a and CoMOF-74. The total alkyne ($C_2H_2 + C_3H_4$)/alkene (C_2H_4) ratio is fixed. JNU-3a fit well with the ideal non-competitive adsorption model (the red dashed line).

https://doi.org/10.1038/s44286-023-00004-2

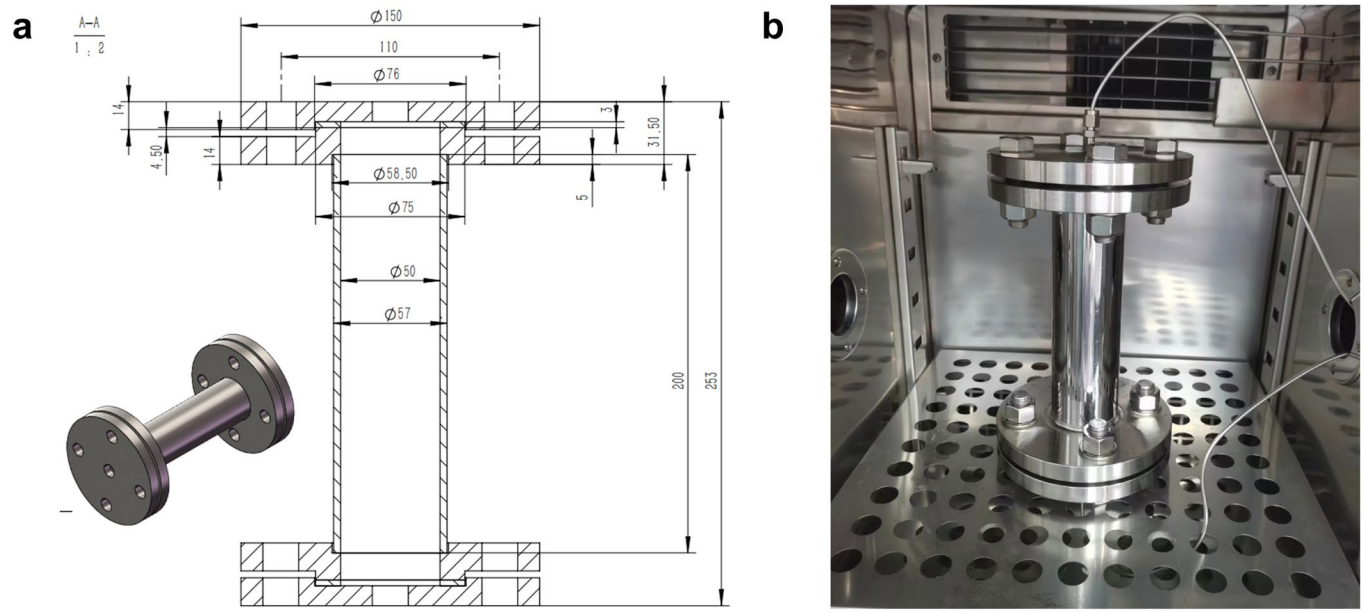

Extended Data Fig. 4 | Dimension of the pilot-scale breakthrough column. (**a**) Construction drawing of the column for the pilot-scale breakthrough. Units are in mm. (**b**) Physical image of the column packed with 107 g of JNU-3a in a thermostatic container.

https://doi.org/10.1038/s44286-023-00004-2

Extended Data Table 1 | Comparison of breakthrough time and productivity

Materials	Breakthrough time (min g^{-1})				Productivity (mL g^{-1})	Purity
	C_2H_4	C_2H_2	C_3H_4	1-C_4H_6		
JNU-3a	24	252	254	279	841.4	99.9995%
CoMOF-74	12	14	560	956	7.8	99.9995%
HKUST-1	28	28	524	1294	–	–
ZJU-74	19	33	63	221	52.5	99.9995%
SIFSIX-3-Ni	11	26	114	65	58.2	99.9995%
ELM-12	11	24	112	116	47.8	99.9995%
SIFSIX-2-Cu-i	14	216	14	14	–	–

Breakthrough time of each component and productivity of high-purity C_2H_4 (99.9995%) on JNU-3a and six contrast MOFs for a C_2H_2/C_3H_4/1-C_4H_6/C_2H_4 (1:1:1:97) mixture (flow rate: 4.0 mL min^{-1}) at 298 K. Productivity was estimated from respective breakthrough curves.

https://doi.org/10.1038/s44286-023-00004-2

Extended Data Table 2 | Small-scale breakthrough and estimated productivity

Feed gas ratio (C_2H_2/C_3H_4/1-C_4H_6/C_2H_4)	Flow rate (mL min^{-1})	Breakthrough time (min g^{-1})				Estimated C_2H_4	
		C_2H_4	C_2H_2	1-C_4H_6	C_3H_4	Productivity (mL g^{-1})	Purity (%)
1:1:1:97	2.0	41	445	449	493	782.9	≥99.9995
1:1:1:97	4.0	24	252	254	279	841.4	≥99.9995
1:1:1:97	6.0	18	175	176	192	912.8	≥99.9995
1:1:1:97	8.0	15	125	124	133	854.7	≥99.9995
1:1:1:97 (50% RH)	4.0	23	233	234	257	814.6	≥99.9995
1:1:1:1	4.0	31	43	46	47	9.9	≥99.9995

Summary of breakthrough experiments on 1.4 g of JNU-3a at different flow rates and feed gas ratios. Productivity was estimated from respective breakthrough curves.

https://doi.org/10.1038/s44286-023-00004-2

Extended Data Table 3 | Pilot-scale breakthrough and gas-cylinder collection

$C_2H_2/C_3H_4/$ 1-C_4H_6/C_2H_4	Collection time		Cylinder weight		Collected C_2H_4		
	Start (min)	End (min)	Empty (g)*	C_2H_4+cylinder (g)	Weight (g)	Productivity (mL g^{-1})**	Purity (%)***
1:1:1:97	50	580	7567.5	7609.6	75.6	565.2	99.9995
2:2:2:94	50	400	7260.0	7303.5	43.5	325.2	99.9995
3:3:3:91	50	350	7183.6	7183.6	36.1	269.9	99.9995
5:5:5:85	50	280	7799.3	7824.4	25.1	187.7	99.9995

Summary of breakthrough experiments on 107 g of JNU-3a for $C_2H_2/C_3H_4/1$-C_4H_6/C_2H_4 mixtures of different ratios (flow rate: 120 mL min^{-1}). *Gas cylinder was vacuumed to ~ 5×10^{-5} mbar using the turbo molecular pump before C_2H_4 collection; **Productivity was calculated from the weight of the collected C_2H_4; ***Purity of the collected C_2H_4 in gas cylinder was determined by gas chromatography.

https://doi.org/10.1038/s44286-023-00004-2

Extended Data Table 4 | Recyclability of pilot-scale breakthrough

Cycles	Collection time		Cylinder weight		Collected C_2H_4		
	Start (min)	End (min)	Empty* (g)	C_2H_4+cylinder (g)	Weight (g)	Productivity** (mL/g)	Purity*** (%)
1	50	580	7567.5	7609.6	75.6	565.2	99.9995
2	50	580	8150.1	8205.6	75.3	563.0	99.9995
3	50	580	8083.9	8140.1	75.8	566.7	99.9995
4	50	580	8175.6	8244.3	75.7	566.0	99.9995
5	50	580	7235.7	7304.3	75.6	565.2	99.9995
6	50	580	7217.6	7287.1	76.6	572.7	99.9995
7	50	580	7799.3	7868.4	76.2	569.7	99.9995
8	50	580	7208.1	7276.4	75.3	563.0	99.9995
9	50	580	7205.5	7274.9	76.5	572.0	99.9995
10	50	580	7187.2	7255.7	75.5	564.5	99.9995
11	50	580	7571.2	7639.1	74.8	559.3	99.9995
12	50	580	7834.2	7905.9	79.0	590.6	99.9995
13	50	580	7183.6	7254.5	78.1	583.9	99.9995
14	50	580	7260.0	7328.9	75.9	567.5	99.9995
15	50	580	7591.5	7662.3	78.0	583.2	99.9995
16	50	580	7567.5	7609.6	75.8	566.7	99.9995
17	50	580	8150.1	8205.6	75.4	563.7	99.9995
18	50	580	8083.9	8140.1	76.8	574.2	99.9995
19	50	580	8175.6	8244.3	75.6	565.2	99.9995
20	50	580	7235.7	7304.3	76.2	569.7	99.9995
21	50	580	7217.6	7287.1	76.2	569.7	99.9995
22	50	580	7799.3	7868.4	75.8	566.7	99.9995
23	50	580	7208.1	7276.4	75.3	563.0	99.9995
24	50	580	7205.5	7274.9	76.1	569.0	99.9995
25	50	580	7187.2	7255.7	75.4	563.7	99.9995
26	50	580	7571.2	7639.1	75.8	566.7	99.9995
27	50	580	7834.2	7909.4	75.2	562.2	99.9995
28	50	580	7183.6	7259.9	76.3	570.5	99.9995
29	50	580	7260.0	7335.7	75.7	566.0	99.9995
30	50	580	7591.5	7667.5	76.0	568.2	99.9995

Summary of 30 cycles of pilot-scale column breakthrough on JNU-3a (107 g) for a $C_2H_2/C_3H_4/1\text{-}C_4H_6/C_2H_4$ (1:1:1:97) mixture (flow rate: 120 mL min^{-1}) at 298 K. *Gas cylinder was vacuumed to ~ 5×10^{-5} mbar using turbo molecular pump before C_2H_4 collection; **Productivity was calculated from the weight of the collected C_2H_4; ***Purity of the collected C_2H_4 in gas cylinder was determined by gas chromatography.